UCLA

UCLA Previously Published Works

Title

Comparative assessment of alternative methods for evaluating the optimality of ground motion intensity measures using woodframe buildings

Permalink

https://escholarship.org/uc/item/2kv963jn

Authors

Dahal, Laxman

Burton, Henry

Handcock, Mark S

Publication Date

2023-10-01

DOI

10.1016/j.soildyn.2023.108084

Copyright Information

This work is made available under the terms of a Creative Commons Attribution License, available at https://creativecommons.org/licenses/by/4.0/

Peer reviewed

eScholarship.org Powered by the California Digital Library
University of California

This version of the article has been accepted for publication, after peer review and is subject to the publisher's terms of use, but is not the Version of Record and does not reflect post-acceptance improvements, or any corrections. The Version of Record is available online at: https://doi.org/10.1016/j.socnet.2023.07.003

Soil Dynamics and Earthquake Engineering

journal homepage: www.elsevier.com/locate/soildyn

Comparative assessment of alternative methods for evaluating the optimality of ground motion intensity measures using woodframe buildings

Laxman Dahal [a,*], Henry Burton [a], Mark S. Handcock [b]

[a] Department of Civil and Environmental Engineering, University of California-Los Angeles, 90095, CA, USA
[b] Department of Statistics, University of California-Los Angeles, 90095, CA, USA

ARTICLE INFO

Keywords:
Intensity measure
Multivariate generalized additive model
GAM
Woodframe buildings
Mutual information
Relative entropy

ABSTRACT

Selection of an optimal ground motion intensity measure (IM) is one of the preliminary yet integral steps in minimizing uncertainty propagation through the probabilistic performance-based earthquake engineering framework. The optimal IM is evaluated and selected based on two widely known evaluation metrics: efficiency and sufficiency. In this study, the univariate regression- and entropy-based methods that are currently available to compute efficiency and sufficiency are presented. More importantly, the existing methods are expanded to account for multivariate relationships between various engineering demand parameters (EDPs), the IM, and the causal parameters. Finally, a comparative assessment of alternative methods is performed based on 10 different IMs and 10 woodframe archetype buildings. The univariate and multivariate methods produce comparable results for the efficiency-based assessment with Sa_{T1} and ASI performing comparably well. Also, for all IMs, both the dispersion and joint entropy are found to be lower in the single-family dwellings (SFDs) compared to the multi-family dwellings (MFDs). This observation can be explained by the higher ductility demands in the latter of the two building types. Similar results are also obtained between the univariate and multivariate entropy-based sufficiency evaluations. In both cases (univariate and multivariate), Sa_{T1} and PGA are the most sufficient IMs for SFDs and MFDs with Sa_{avg} also performing well for the MFDs.

1. Introduction

In modern performance-based earthquake engineering (PBEE) [1], seismic hazard analysis is systematically and probabilistically associated with loss estimation by utilizing the total probability theorem:

$$\lambda(\mathrm{DV}) = \iiint \mathrm{G}\langle \mathrm{DV}|DM\rangle dG\langle DM|\mathrm{EDP}\rangle dG\langle \mathrm{EDP}|\mathrm{IM}\rangle d\lambda(\mathrm{IM}) \quad (1)$$

where $\lambda(\mathrm{DV})$ and $\lambda(\mathrm{IM})$ are the annual exceedance rates for the decision variable of interest and ground motion intensity measure (IM), respectively. The "triple integral" also utilizes the conditional probability of exceeding (i) the decision variable given the damage measure (DM), $\mathrm{G}\langle \mathrm{DV}|DM\rangle$, (ii) the damage measure given the engineering demand parameter (EDP), $G\langle DM|\mathrm{EDP}\rangle$, and (iii) EDP given an IM, $G\langle \mathrm{EDP}|\mathrm{IM}\rangle$. The latter of the three conditional probabilities is obtained from probabilistic seismic demand analysis (PSDA), which computes the structural response, ideally using nonlinear response history analyses. The formulation shown in Eq. (1) is based on an underlying assumption that the EDP of interest is conditionally independent of the ground motion causal parameters such as magnitude (M) and source-to-site distance (R). Preferably, all the predictor variables used in the ground motion model (GMM) (e.g., shear-wave velocity (Vs_{30}), fault type, average depth (Z_{TOR}), average dip angle (δ)) would be included as causal parameters. In this study, only M and R are discussed because their contributions are dominant in the GMM and seismic hazard deaggregation [2,3]. Hereafter, the term "causal parameters" jointly refers to M and R.

The independence of the conditional distribution of an EDP with respect to the causal parameters can be regarded as a "weak" assumption in the sense that it is not absolutely essential in the PBEE framework. In other words, the dependence on the causal parameters can be explicitly considered by conditioning the EDP on IM, M, and R instead of just the IM. As highlighted in Luco and Cornell [2] (Equation 12), the explicit consideration of the causal parameters in Eq. (1) increases the computational cost as one has to integrate over all the causal parameters in addition to the triple integral, but it is within the realm of possibility. However, while possible, the explicit consideration of causal parameters is not always practical. This approach would require the suite of ground motion records to be consistent with $G\langle R, M|\mathrm{IM}\rangle$, which essentially means that the selected records need to come from the earthquake events that govern the hazard at all the IM levels.

* Corresponding author.
E-mail address: laxman.dahal@ucla.edu (L. Dahal).

https://doi.org/10.1016/j.soildyn.2023.108084
Received 12 February 2023; Received in revised form 9 June 2023; Accepted 10 June 2023
0267-7261/© 2023 Elsevier Ltd. All rights reserved.

Realistically, ground motion suites that are consistent with respect to the causal parameters would be rare because it is unlikely that an event with specific characteristics (e.g., M, R) would dominate the IMs at all hazard levels. It is noted that the consistency issue can be countered by selecting site- and intensity-specific ground motions. The targeted ground motion selection, however, might not be a universal solution to this consistency issue because in applications such as regional studies, cloud analysis might be preferred. The bottom line is that the explicit consideration of conditional dependence imposes an immense limitation on the PBEE framework. Hence, to ease the limitation and increase computational viability, the PBEE framework adopts a simplifying conditional independence assumption. The assumption emphasizes the identification, selection, and evaluation of an "optimal" IM which is the focus of the paper.

Recognizing the importance of IM selection in quantifying and propagating uncertainty in the PBEE methodology, there has been a body of research work investigating different facets of the optimality of an IM. The most widely accepted metrics to assess the effectiveness of an IM are "efficiency" and "sufficiency"[2,4]. Efficiency is a measure of an IM's ability to define the relationship between seismic response and hazard with minimal dispersion. In other words, the efficiency of an IM quantifies the uncertainty of the conditional structural response (EDP | IM). On the other hand, an IM is said to be sufficient if the conditional distribution of the EDP of interest is independent of the causal parameters. This serves as an indication that the IM alone can adequately estimate the structural response with no additional information from the causal parameters. The earliest attempts to quantify efficiency and sufficiency were based on ordinary least squares (OLS) regression (referred to as the "traditional" approach henceforth). Specifically, the conditional distribution of the response demands is estimated by regressing the EDP against the IM. The EDPs are obtained from nonlinear response history analysis (NRHA) under a suite of ground motion records. The standard error obtained from the OLS is then taken as the efficiency measure. The residual of the first OLS model is further regressed on the causal parameter in a one-at-a-time fashion to determine the sufficiency of the IM. The sufficiency criterion relies on statistical significance testing under a pre-specified significance level (α). If the regression coefficient corresponding to the causal parameter is statistically insignificant at the desired confidence level (p-value > α), the IM is deemed sufficient. Other metrics such as "predictability", "scaling robustness", "practicality", and "proficiency" [5,6] have also been proposed, but for generality, this study only focuses on efficiency and sufficiency as the primary evaluation metrics.

An intrinsic assumption in the one-parameter linear model approach to quantifying efficiency is that the EDPs are independent and thus follow a univariate distribution. This assumption, which is usually made as a matter of convenience, has three primary implications: (1) intra-EDP joint distribution (e.g., EDP profile along the story height) cannot be considered, (2) inter-EDP (e.g., peak story drift ratio (SDR) and peak floor acceleration (PFA)) dependence and interactions cannot be incorporated, and (3) multivariate effects of multiple causal parameters cannot be addressed. It is well understood that the nonlinear behavior of a structure under dynamic loading is a consequence of complex interactions between displacements, velocities, and accelerations of structural and nonstructural components. It is a common practice to assume that EDPs jointly follow a lognormal distribution [1]. Notably, in the PBEE framework, the Monte Carlo algorithm is used to simulate jointly lognormal demand samples to assess losses. The simulated demand samples include direction-dependent EDPs and their profiles along the building height. This enables the framework to conveniently consider intra- and inter-EDP dependence. However, in IM evaluation studies, the optimality of an IM has been investigated assuming that the EDPs follow independent lognormal distributions. Although the majority of prior IM studies [7–9] have used the maximum value of the EDP profile along the story height, a limited number of studies have utilized three-dimensional models [10] and considered the EDP profile [11] in analyzing the effectiveness of an IM. Recent studies have also proposed an entropy-based evaluation metric for site-specific risk assessment [12,13]. Du and Padgett [13] proposed a joint entropy-based procedure to evaluate IMs by considering the multivariate distribution of the demand parameters for a bridge structure. However, to the best of our knowledge, there has not been a similar study for buildings where multiple EDPs are considered.

This paper is guided by two primary motivations: (1) to perform a comparative analysis of the currently available methods and (2) to advance the current methods by explicitly considering multivariate relationships in building structural responses. Fig. 1 summarizes a host of existing and new methods covered throughout this paper. First, we present the OLS-based efficiency assessment approach and the joint entropy-based measure as alternative criteria. The joint entropy approach was originally proposed by Du and Padgett [13] as a singular measure of the optimality of an IM. Under the assumption that EDPs are jointly lognormal, we implement a multi-target generalized additive model (GAM) [14] with smooth functions to effectively capture the multivariate and nonlinear relationships between the EDPs and IM. Ultimately, we use the estimated covariance matrix to assess the efficiency of the IM based on joint entropy. Similarly for sufficiency, we start by presenting the univariate OLS approach. Staying within the significance testing domain, we also implement a multivariate GAM to determine sufficiency while accounting for the multivariate relationships within and between EDPs, and causal parameters. We present the relative sufficiency measure as an alternative approach for both the univariate and multivariate cases. The relative sufficiency measure presented here is inspired by two previous studies [12,15]. Finally, we implement these approaches on a set of 10 residential woodframe buildings consisting of four single-family dwellings (SFD) and six multi-family dwellings (MFD). Although there has been a large body of research on IM evaluation for a variety of structures, woodframe buildings have garnered much less attention. Heresi and Miranda [16] investigated the efficiency of 10 different IMs for regional-based risk assessment of low-rise woodframe buildings. However, the sufficiency criterion was not considered in their study. To the best of our knowledge, this study is the first of its kind to evaluate IMs for woodframe buildings using entropy-based efficiency and sufficiency measures.

2. Quantifying IM optimality

We perform a comparative assessment of IM optimality using the various metrics shown in Fig. 1. Acknowledging the availability of other evaluation metrics (e.g., robustness, predictability, etc.), this paper focuses on efficiency and sufficiency. In the subsequent subsections, a wide variety of methods ranging from univariate OLS to multivariate entropy-based techniques are discussed as measures to evaluate the effectiveness of an IM.

2.1. Methods to quantify the efficiency

The efficiency of an IM is a measure of the dispersion of an estimated EDP in PSDA. It is one of the most straightforward evaluation metrics that reflects the predictive performance of the demand model based on the measure of uncertainty in the conditional distribution of the EDP.

2.1.1. Univariate OLS-based efficiency

Historically, efficiency has been assessed by evaluating the residual standard error obtained from one-parameter regression of the EDP against the IM [2,17]. The functional form of the univariate log–log linear model is shown in Eq. (2)

$$\ln \mathrm{EDP}|\mathrm{IM} = \beta_0 + \beta_1 \cdot \ln \mathrm{IM} \ + \ln(\epsilon|\mathrm{IM}) \tag{2}$$

where $\ln(\epsilon|\mathrm{IM})$ is a normally distributed noise term with mean zero and standard deviation $\sigma_{\mathrm{EDP|IM}}$, β_0 is an intercept, and β_1 is a slope in log

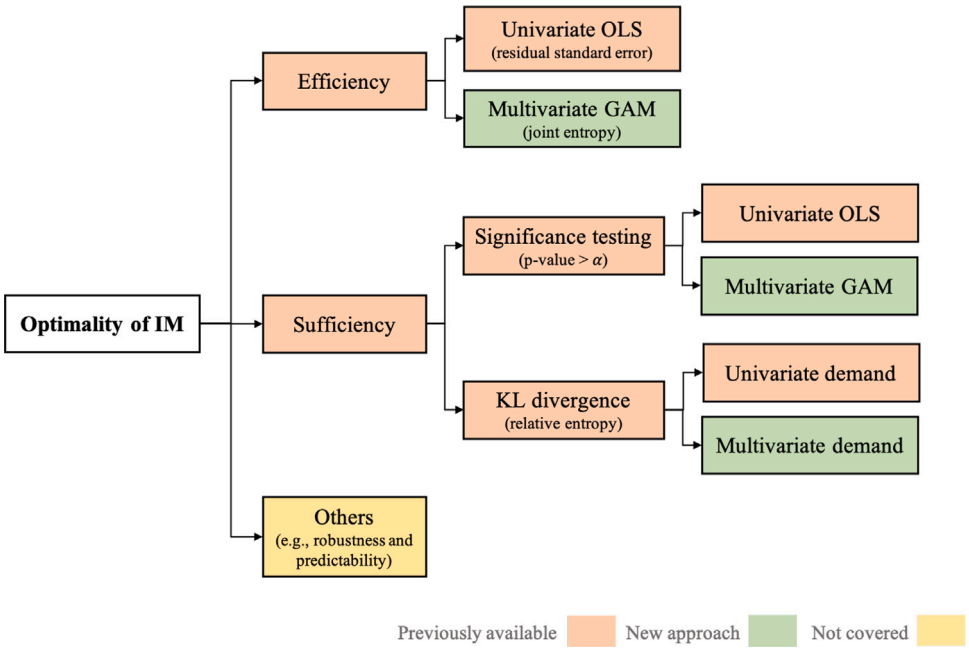

Fig. 1. Summary of the various methods used to evaluate the effectiveness of IM.

scale. The use of the log–log model ensures the validity of the normality assumption since the EDP and IM are expected to be linearly related in log space [17,18]. The normality enables the residual standard error (RSE), $\sigma_{\mathrm{EDP|IM}}$, can be directly used as a measure of efficiency. The RSE in Eq. (2) does not need to be transformed to log space because it is an estimate of the standard deviation of the residuals in log space. It is evident from Eq. (2) that an efficient IM would require fewer NRHAs to estimate the structural response as compared to one that is less efficient.

2.1.2. Multivariate entropy-based efficiency

The OLS model is limited to a univariate relationship between the EDP and IM. In reality, different EDPs within a structure follow a joint distribution. Additionally, the relationship between the log-transformed EDP and IM is often more complex than simply linear. To account for this nonlinear multivariate relationship, a multi-target GAM model is proposed. The GAM is a smooth extension of the generalized linear model (GLM) where the linear form in GLM is replaced by a sum of smooth functions [14]. These smooth functions are represented via splines and inferred from the data. It is highly flexible and designed to capture the nonlinear relationship between the response and predictor variable via the smooth function ($s(\cdot)$). The smooth functions for each response-predictor variable pair are estimated simultaneously via the maximized penalized likelihood method [19]. Ultimately, the smooth functions are all added together to formulate a simple yet powerful GAM model as shown in Eq. (3). For detailed mathematical information on the algorithm, the reader is referred to Hastie and Tibshirani [14] and Friedman and Stuetzle [19]. The model can be expressed as:

$$\ln \mathbf{EDP}|\mathrm{IM} = \mathbf{s_1}(\ln \mathrm{IM}) + \ln(\epsilon|\mathrm{IM}) \tag{3}$$

In Eq. (3), $\ln \mathbf{EDP}$ is a vector of EDPs within the structure, $\mathbf{s}(\cdot)$ is a vector of non-parametric smooth functions, and $\ln(\epsilon|\mathrm{IM})$ is a multivariate normal error distribution with mean zero and diagonal covariance matrix. The output of the fitted model is RSE in the form of a covariance matrix ($\boldsymbol{\Sigma}$). To properly account for the covariances between all the EDPs, the concept of joint entropy from information theory is leveraged. The use of joint entropy in the context of IM evaluation was first proposed by Du and Padgett [13]. However, in this study, we reframe entropy as an alternative measure of efficiency because it is a measure of "surprise" or uncertainty in a random variable's possible outcomes. Assuming that the EDPs roughly follow a multivariate normal distribution in log space [1], their joint entropy can be computed using the analytical solution in Eq. (4). An IM is regarded as the most efficient if it has the lowest joint entropy among the IMs that are considered. Intuitively, the most efficient IM induces the least uncertainty in PSDA.

$$h\left(\langle \ln \mathrm{EDP}_1|\mathrm{IM}\rangle, \langle \ln \mathrm{EDP}_2|\mathrm{IM}\rangle, \ldots, \langle \ln \mathrm{EDP}_n|\mathrm{IM}\rangle\right) = \frac{1}{2}\log\left((2\pi e)^d \det(\boldsymbol{\Sigma})\right) \tag{4}$$

where $\det()$ is the determinant of a matrix. It is noted that this formulation assumes the bias to be zero.

2.2. Methods to quantify sufficiency

The idea of sufficiency follows from the assumed independence between the structural response and the ground motion causal parameters after conditioning on the IM. At its core, sufficiency is a measure of the simplifying assumption that an IM is adequate in defining the conditional distribution of the EDP without any additional information from the causal parameters. A sufficient IM also simplifies the ground motion selection process because the suite of selected records does not necessarily need to be consistent with the causal parameters at each hazard level. In other words, a sufficient IM is less reliant on the decisions made during the ground motion selection process. Thus, it can be argued that a sufficient IM results in a more robust EDP distribution [9,16].

2.2.1. Univariate OLS-based significance testing

Traditionally, the sufficiency of an IM is determined via a null hypothesis significance test characterized by a p-value [2]. A multiple linear regression model outlining the relationship between an EDP, IM, and a causal parameter is formulated for hypothesis testing. Equivalently, the normally distributed residuals ($\ln(\epsilon|\mathrm{IM})$ obtained from Eq. (2) can also be regressed on the causal parameter directly. The two variations of regressions are highlighted in Eq. (5) where x represents a causal parameter (either M or R) considered individually. If the observed p-value for the causal parameter (i.e. p-value of β_2 in Eq. (5a) or β_1 in Eq. (5b)) is higher than the pre-defined significance level (typically $\alpha = 5\%$), then the null hypothesis cannot be rejected, suggesting that the IM is sufficient. However, a p-value lower than the specified

threshold signifies that the causal parameter is statistically significant in establishing the conditional distribution of the EDP. The statistical significance of the causal parameter makes an IM insufficient because it implies that the information from the causal parameter is essential in defining the structural response. Interested readers are referred to the following literature [2,5] for a more elaborate description of hypothesis testing and sufficiency.

$$\ln \mathrm{EDP} = \beta_0 + \beta_1 \cdot \ln \mathrm{IM} \ + \beta_2 \cdot x + \ln(\epsilon|\mathrm{IM}, x) \tag{5a}$$

$$\ln(\epsilon|\mathrm{IM}) = \beta_0 + \beta_1 \cdot x + \ln(\epsilon|\mathrm{IM}, x) \tag{5b}$$

2.2.2. Multivariate GAM-based significance testing

As discussed earlier, the OLS-based sufficiency model disregards the nonlinear and multivariate relationship between the conditional structural response distribution and causal parameters. In GAMs, a scalar IM is derived based on interdependence between various causal parameters. Thus, to render an IM sufficient, a multivariate relationship between the causal parameters should also be considered. The multi-target multivariate GAM presented in Eq. (3) can be used to consider the causal parameters as follows

$$\ln \mathbf{EDP}|\mathrm{IM} = \mathbf{s_1}(\ln \mathrm{IM}) + \mathbf{s_2}(\ln M) + \mathbf{s_3}(\ln R) + \ln(\epsilon|\mathrm{IM}, M, R) \tag{6}$$

where, $\ln \mathbf{EDP}$ is a vector of EDPs, $\mathbf{s_i}(\cdot)$'s are vectors of non-parametric smooth functions and $\ln(\epsilon|\mathrm{IM})$ is the jointly distributed error. Like the OLS-based significant testing, the sufficiency of an IM is determined based on the significance of the smooth terms for M and R. The GAM can be viewed as a non-parametric extension of OLS as it provides flexibility to consider multivariate EDPs and multivariate causal parameters. Eq. (6) is a highly flexible formulation that can be simplified by only considering one causal parameter at a time. On the other hand, it can also be modified to account for two-way or three-way interactions between the IM and the causal parameters as described in Eq. (7)

$$\ln \mathbf{EDP}|\mathrm{IM} = \mathbf{s_1}(\ln \mathrm{IM}, \ln M) + \mathbf{s_2}(\ln \mathrm{IM}, \ln R) + \ln(\boldsymbol{\epsilon}|\mathrm{IM}, M, R) \tag{7a}$$

$$\ln \mathbf{EDP}|\mathrm{IM} = \mathbf{s_1}(\ln \mathrm{IM}, \ln M, \ln R) + \ln(\boldsymbol{\epsilon}|\mathrm{IM}, M, R) \tag{7b}$$

2.2.3. Univariate entropy-based sufficiency

The GAM-based sufficiency measure addresses the need to consider multivariate relationships within and between the EDPs and causal parameters. It is noted that Kazantzi and Vamvatsikos [11] proposed dispersion-based metrics that negate subjectivity while staying within the realm of OLS. The idea is to compare the mean and maximum dispersion explained by the causal parameters to determine sufficient IM. This paper uses the Kullback–Leibler divergence (commonly known as KL divergence) as an alternative measure to quantify the degree of sufficiency. KL divergence (equivalently, relative entropy) has previously been implemented as a measure of sufficiency [12,15]. In particular, Dhulipala et al. [12] used KL divergence to calculate total information gain by comparing the site-consistent conditional distribution of an IM with and without including a causal parameter i.e. $f_{R\ or\ M}(\mathrm{IM}\ |\mathrm{EDP} > \mathrm{edp})$ and $f(\mathrm{IM}\ |\mathrm{EDP} > \mathrm{edp})$. The conditional distribution of an IM is computed by applying Bayes rule to the probability of demand exceedance ($P(\mathrm{EDP} > \mathrm{edp}|\mathrm{IM})$). The transformation of the probability of demand exceedance into the conditional distribution of the IM warrants hazard deaggregation. However, since the assumed context in this study is a site-agnostic regional-based assessment, the KL divergence can be computed between the conditional distributions without seismic hazard deaggregation.

Suppose, P and Q are, respectively, the distributions of EDP conditioned on IM with and without the causal parameter (x). Let $p(\ln \mathrm{EDP}|\mathrm{IM})$ and $q(\ln \mathrm{EDP}|\mathrm{IM}, x)$ be the corresponding densities of P and Q. The causal parameter can be considered one-at-a-time (either M or R) or all-at-once (M and R). Given the univariate conditional distributions, P, and Q, the KL divergence is computed using Eq. (8). The KL divergence effectively becomes a sufficiency measure that quantifies the degree to which an IM can render the conditional distribution of the EDP independent of the causal parameter.

$$D_{\mathrm{KL}}(P \parallel Q) = \int p(\ln \mathrm{EDP}|\mathrm{IM}) \log\left(\frac{p(\ln \mathrm{EDP}|\mathrm{IM})}{q(\ln \mathrm{EDP}|\mathrm{IM}, x)}\right) d \ln \mathrm{EDP} \tag{8}$$

Under the assumption that P and Q are normally distributed, the KL divergence formulation in Eq. (8) simplifies to the analytical solution given by Eq. (9). For each IM, the KL divergence between the conditional distribution of the EDP with and without the causal parameter are compared. The IM with the least KL divergence indicates that the causal parameters contribute the smallest amount of additional information in defining the conditional distribution of the EDP (i.e., $P \approx Q$) and is, hence, deemed the most sufficient.

$$D_{\mathrm{KL}}(P \parallel Q) = \log\frac{\sigma_Q}{\sigma_P} + \frac{\sigma_P^2 + (\mu_P - \mu_Q)^2}{2\sigma_Q^2} - \frac{1}{2} \tag{9}$$

2.2.4. Multivariate entropy-based sufficiency

The relative entropy-based measure presented in subsection Section 2.2.3 is an alternative to the significance testing-based approach within the univariate EDP space. In this subsection, we present a generalizable method to consider the multivariate conditional distributions of EDPs with and without causal parameters. Particularly, we compute the KL divergence between residuals obtained by regressing $\ln \mathrm{EDP}$ on $\ln \mathrm{IM}$ (i.e., $\ln(\epsilon|\mathrm{IM})$ from Eq. (2)) and residuals obtained by regressing $\ln \mathrm{EDP}$ on $\ln \mathrm{IM}$ and the causal parameters (i.e., $\ln(\epsilon|\mathrm{IM}, x)$ from Eq. (5)). The distribution of the residuals is preferred over the predicted conditional distribution of the EDP because the former follows a normal distribution which validates the use of the analytical KL divergence formulation in Eq. (9). The results of the normality tests on the residuals have been provided as supplementary material [20].

Another advantage of using residuals is the flexibility to incorporate multivariate EDP distributions. Consistent with the FEMA P-58 framework, the log-transformed SDR and PFA (or equivalently their residuals from Eq. (2)) are assumed to follow a multivariate normal distribution [1]. To compute the KL divergence between two jointly normal distributions, let $\mathcal{N}_0 \sim \mathcal{N}(\boldsymbol{\mu}_0, \boldsymbol{\Sigma}_0)$ be the joint conditional distribution of the EDPs without causal parameters and $\mathcal{N}_1 \sim \mathcal{N}(\boldsymbol{\mu}_1, \boldsymbol{\Sigma}_1)$ be the joint conditional distribution of the same EDPs with the causal parameter. The generic formulation of KL divergence is simply an extension of Eq. (8) but for normally distributed multivariate distributions, there is a closed-form solution as show below

$$D_{\mathrm{KL}}(\mathcal{N}_0 \parallel \mathcal{N}_1) = \frac{1}{2}\left\{\mathrm{tr}\left(\boldsymbol{\Sigma}_1^{-1}\boldsymbol{\Sigma}_0\right) - d + (\boldsymbol{\mu}_1 - \boldsymbol{\mu}_0)^T\boldsymbol{\Sigma}_1^{-1}(\boldsymbol{\mu}_1 - \boldsymbol{\mu}_0) + \log\frac{\det\left(\boldsymbol{\Sigma}_1\right)}{\det\left(\boldsymbol{\Sigma}_0\right)}\right\} \tag{10}$$

where $\mathrm{tr}()$ is the trace of a matrix, $\boldsymbol{\mu}_0$ and $\boldsymbol{\mu}_1$ are the mean vectors, d is the dimension of $\mathcal{N}_0$ and $\mathcal{N}_1$, $\boldsymbol{\Sigma}_0$ and $\boldsymbol{\Sigma}_1$ are the correlation matrices. For illustration, suppose SDR and PFA are jointly lognormal. The two multivariate distributions $(\mathcal{N}_0, \mathcal{N}_1)$ then might take the following functional forms: $\mathcal{N}_0 \sim \mathcal{N}([\mu_{\ln SDR|\mathrm{IM}}, \mu_{\ln PFA|\mathrm{IM}}], \boldsymbol{\Sigma}_0)$ and $\mathcal{N}_1 \sim \mathcal{N}([\mu_{\ln SDR|\mathrm{IM},x}, \mu_{\ln PFA|\mathrm{IM},x}], \boldsymbol{\Sigma}_1)$. The KL divergence between $\mathcal{N}_0$ and $\mathcal{N}_1$ quantifies the amount of information gained due to the inclusion of a causal parameter (x) in $\mathcal{N}_1$. Identical to the univariate case, the IM with minimal KL divergence is regarded as the most sufficient IM.

3. Ground motion records and intensity measures

For the IM evaluation, 826 pairs of site-agnostic ground motion records from 63 crustal earthquakes recorded by far-field strong motion stations are used. The records were utilized by Heresi and Miranda [16] to evaluate IMs for low-rise woodframe buildings at a regional scale. The authors originally selected 831 record pairs but due to periodic updates of the PEER NGA-West2 ground motion database [21], only 826 pairs of records were available for download at the time of

this study. The details about the entire suite of records can be found in Heresi et al. [22]. The 826 ground motion pairs were recorded between 1942 and 2011 and have a minimum, average, and maximum moment magnitude of 5.1, 6.8, and 7.9 respectively. Similarly, the suite of records has a mean Joyner-Boore distance of 77.2 km while the minimum and maximum distances were 0, and 315.9 km, respectively. The records correspond to NEHRP site class D with 266.7 m/s average shear wave velocity. Fig. 8 in Appendix A shows additional ground motion information such as the pairwise relationship between the causal parameters and response spectrum of the suite of selected ground motions.

The unscaled acceleration histories are used to avoid the possibility of bias being induced due to scaling. Large scale factors have been found to produce a biased estimation of structural response in short-period buildings [23,24]. In the PBEE framework, it is customary to scale ground motions to match pre-specified spectral acceleration levels. Moreover, IM-based ground motion scaling would likely produce results that are biased for that specific IM. We acknowledge that the use of unscaled records also has its limitations (i) ground motions with higher intensity levels are less common, and (ii) two ends of IM distribution might be dominated by a highly specific set of causal parameters. A number of studies [23–25] have explored the idea of the capped scale factor to minimize bias induced due to amplitude scaling. The limitations posed by unscaled ground motion are viewed as a trade-off to minimizing bias.

3.1. Intensity measures

Over the last two decades, a wide range of IMs has been proposed, from vector IMs to advanced frequency-based IMs [7,16,26–28]. However, in this study, a total of 10 IMs that range from acceleration-based to displacement-based are considered. Each ground motion pair consists of two horizontal time series records (H1 and H2) with their respective orientation in which the acceleration was recorded. The 50th percentile rotated spectrum (RotD50) is computed [29] by rotating the spectrum through 180 degrees and taking the 50th percentile. The details of the 10 IMs are presented as follows:

1. **Spectral acceleration (Sa_{T1}):** The Sa_{T1} represents the maximum acceleration that a ground motion will cause in a linear oscillator with a specified period (oftentimes the same fundamental period as a building) and damping level. An accurate representation is pseudospectral acceleration which is given by a product of spectral displacement with the squared natural frequency. As discussed in Baker and Cornell [30], the difference between the spectral and pseudospectral acceleration is negligible which is why the term "spectral acceleration" is used hereafter. The spectral accelerations for all 826 ground motions are computed using a Python library that employs the discrete fast Fourier transformation [31].
2. **Peak ground acceleration (PGA):** The PGA is a period-independent measure of the maximum acceleration recorded during an earthquake. It is the maximum absolute acceleration from the time series.
3. **Peak ground velocity (PGV):** The PGV is the maximum velocity of an earthquake ground motion. PGV is computed by taking the first-order integral of an acceleration time series with respect to time.
4. **Cumulative absolute velocity (CAV):** The CAV [32] is one of the frequently studied IMs that is intended to capture the cumulative effects of ground motion shaking. Mathematically, it is defined as the integral of the absolute value of the acceleration, $CAV = \int_{t_0}^{t_{max}} |a(t)|dt$.
5. **Average spectral acceleration (Sa_{avg}):** The Sa_{avg} is the geometric mean of the spectral acceleration for a range of periods $[T_{min}, T_{max}]$ [9,33,34]. Sa_{avg} aims to capture ground motion effects in cases where the structure responds to a range of frequencies due to period elongation during inelastic response or multi-modal response. Conceptually, it is an ideal IM for regional assessment where the fundamental periods of the buildings are bounded within T_{min} and T_{max}. It is computed as,

$$Sa_{avg}(T_{min}, T_{max}) = \left[\prod_{t=T_{min}}^{T_{max}} Sa(T=t)\right]^{\frac{1}{N}} \tag{11}$$

   where N is the total number of periods between equally spaced values between T_{min} and T_{max}. The period range is taken as $[0.1T_{1,min}, 2T_{1,max}]$ where $T_{1,min}$ and $T_{1,max}$ are the minimum and maximum fundamental periods among 10 archetypes.
6. **Spectrum intensity (SI):** The SI, also commonly known as response spectrum intensity is computed by taking the area under the velocity spectrum curve between periods 0.1 and 2.5 s [35]. SI was proposed to characterize the response of a broad class of structures whose fundamental periods are expected to be between 0.1 and 2.5 s. SI is computed using $SI = \int_{0.1}^{2.5} SV(T)dT$ where, $SV(T)$ is the spectral velocity at period, T.
7. **Acceleration spectrum intensity (ASI):** The ASI is conceptually similar to SI, but it is most widely used as an intensity measure in stiff structures (e.g., dams) where the first-mode fundamental period is typically less than 0.5 s [36]. Although residential woodframe buildings are not stiff by design, ASI, in principle, would be a very appropriate measure considering the fundamental period typically ranges from 0.1 to 0.5 s. To the best of our knowledge, ASI has not been considered in the IM optimality literature discussed above. It is computed by, $ASI = \int_{0.1}^{0.5} Sa(T)dT$
8. **Displacement spectrum intensity (DSI):** The DSI is a spectral displacement-based measure that is intended to capture the impact of the long-period content of a ground motion on structural performance [37]. It is computed as the area under the spectral displacement curve between periods of 2 and 5 s using $DSI = \int_{2}^{5} SD(T)dT$ where $SD(T)$ is the spectral displacement at period T.
9. **Significant duration (DS):** The DS is a measure of the cumulative energy dissipated by the acceleration time series. The energy dissipation, also commonly known as Arias Intensity (AI) [38], is captured by integrating the squared acceleration time series, i.e., $AI(t) = \int_0^{t_{max}} a(t)^2 dt$. DS defines the time a ground motion takes to dissipate a pre-specified amount of energy. For instance, $DS_{5\text{-}95}$ is the time it takes to dissipate 90% of the total energy $(AI(t)/AI_{max})$ between 5% and 95% intervals. The two most widely used duration ranges, $DS_{5\text{-}75}$ and $DS_{5\text{-}95}$ are considered as IMs.

4. Building description

A total of 10 woodframe building archetypes are used. They were developed as a part of the FEMA P-2139-2 project [39] to study the short-period (fundamental period < 0.5 s) wood light-frame building performance paradox. The paradox was a contradictory seismic collapse performance obtained from numerical simulations that did not support the actual performance observed during historical earthquakes. Based on the numerical models, short-period buildings were believed to have a higher collapse risk than long-period buildings. However, the observed collapse risk from historical earthquakes was much lower than what was predicted by structural response simulation. To address this discrepancy, enhanced numerical models were employed in a bid to create a realistic representation of the observed performance. The FEMA P-2139-2 project studied 28 baseline archetypes that comprised

Table 1
Summary of the basic building information for the set of considered archetypes.

Archetype ID	No of stories	Seismic weight(kips)	Design level	SDC	C_s	Plan dimensions (ft)	Story height (ft)
SFD1B	1	[51]	High	D_{max}	0.154	32 × 48	10
SFD3B	1	[51]	Very high	1.5 × D_{max}	0.231	32 × 48	10
SFD2B	2	[53, 70]	High	D_{max}	0.154	32 × 48	10
SFD4B	2	[53, 70]	Very high	1.5 × D_{max}	0.231	32 × 48	10
MFD1B	1	[141]	High	D_{max}	0.154	48 × 96	10
MFD4B	1	[141]	Very high	1.5 × D_{max}	0.231	48 × 96	10
MFD2B	2	[182, 144]	High	D_{max}	0.154	48 × 96	10
MFD5B	2	[182, 144]	Very high	1.5 × D_{max}	0.231	48 × 96	10
MFD3B	4	[237, 237, 237, 149]	High	D_{max}	0.154	48 × 96	10
MFD6B	4	[237, 237, 237, 149]	Very high	1.5 × D_{max}	0.231	48 × 96	10

commercial (COM), single-family dwellings (SFD), and multi-family dwellings (MFD) with either one, two, or four-story variants.

Table 1 outlines the naming convention and general design information about the archetypes. As shown, the 10-building set contains four SFDs and six MFDs. The buildings are designed for "High" and "Very high" seismic design levels. The "High" design level corresponds to the seismic design category (SDC) D_{max} with a seismic response coefficient C_s value of 0.154. It is intended to mimic the seismic demand produced by MCE_R-level ground motions in regions with high seismicity. Table 1 contains the complete set of response coefficients, floor layouts, and story heights of all the archetypes. The interested reader is referred to the FEMA P-2139-2 document [39] which contains design details including the graphical renderings of the archetypes.

4.1. Numerical modeling and analysis

Three-dimensional (3D) OpenSees [40] models are constructed for all 10 archetypes where X- and Z- axes are used to denote the two horizontal directions. In FEMA P-2139-2, a modified seismic analysis of woodframe structures (SAWS) [41] hysteresis material model is used to capture the nonlinear behavior of different components of the building including the light-frame wood shear wall and nonstructural partitions. The 10-parameter SAWS material model is limited in its ability to capture the residual strength and stiffness of the panels. The residual capacity is one of the key contributing factors in determining the performance of structures that undergo large deformations (e.g., woodframe buildings). To overcome these shortcomings, a versatile 22-parameter Pinching4 hysteresis model is used. Originally developed to model the highly nonlinear behavior of two-dimensional beam–column joints [42], the Pinching4 hysteretic model has since been adopted to model the cyclic degradation of strength and stiffness in a variety of components such as the cripple wall, light-frame wood wall, and steel moment frames [43–45].

4.1.1. Pinching4 material parameter calibration

One of the drawbacks of using the Pinching4 model is that the parameters are not readily available in the literature as compared to the SAWS parameters. The 22-parameter Pinching4 hysteresis model is composed of eight backbone and 14 cyclic parameters that can be calibrated based on either the experimental data or the SAWS parameters. In this study, the pinching4 parameters for wood shear walls are calibrated based on the SAWS hysteresis model. The calibration process involves two distinct steps: backbone curve fit (backbone parameters calibration) and hysteresis pseudo-energy match (cyclic parameters calibration). The backbone parameters (e.g., initial stiffness, peak strength, drift at peak strength, etc.) are simply extracted based on the backbone curve presented in the FEMA P-2139-2. For cyclic parameters, two single-degree-of-freedom (SDOF) OpenSees models are created representing the SAWS and Pinching4 material model, respectively. The SAWS model directly uses the SAWS parameters as reported in FEMA P-2139-2. The Pinching4 model utilizes eight known backbone parameters and 14 best-guess cyclic parameters which are iterated until the pseudo-energy matches closely. The models are then subjected to a quasi-static cyclic loading protocol and the resulting force–deformation curve is generated as shown in Fig. 2(a). Fig. 2(b) compares the energy dissipation between the SAWS (red) and Pinching4 (blue) models. The near-identical curves indicate that the SAWS and calibrated Pinching4 material model are equivalent. In parameter calibration, it is standard to compare the strength loss only up to 40% strength to declare a "good fit". Interested readers are referred to Welch et al. [43] for a more thorough description of the calibration process and criteria. Fig. 2 demonstrates the Pinching4 parameter calibration of a wood shear wall assembly labeled "OSB-Med" in FEMA P-2139-2.

4.2. Nonlinear static analysis

To verify the OpenSees models, Table 2 compares the results from nonlinear static analysis against the values documented in the FEMA P-2139-2 report.

As outlined in Table 2, the fundamental periods for all 10 archetypes are in alignment with the FEMA P-2139 results. On average, the periods differ by 7% which is expected when two entirely different modeling software are used (Timber3D in FEMA P-2139 and OpenSees in this study). Similarly, the normalized base strengths (maximum base shear normalized by the seismic weight) are comparable with an average difference of 9%. The ultimate drift capacity (drift at 80% peak strength) was found to differ by 24% on average. Again, considering the fact that two different hysteresis models were used to represent the cyclic strength degradation, a 24% variability is considered acceptable. The table also reports the displacement ductility demand [46] as a measure of inelastic deformation experienced by the building under dynamic excitation. Note that the ductility demand was not computed in the FEMA P-2139-2 report.

4.3. Nonlinear dynamic analysis

After verifying the nonlinear static analysis results, site-agnostic NRHAs are performed by subjecting the 3D models to the full suite of 826 ground motion pairs. Two sets of structural responses are generated. First, the two horizontal acceleration time series are applied simultaneously assuming H1 and H2 of the ground motion orientation correspond to the X- and Z-direction of the model, respectively. Consequently, the second set of responses is obtained by subjecting the model to orthogonally rotated record pairs. The two sets of orientation-dependent responses are combined into one by computing the geometric mean. The output of the NRHA is an orientation-independent EDP (SDR and PFA) profile along the story height in both the X- and Z-direction. The EDP profile for a two-story SFD and a four-story MFD is highlighted in Appendix B. Additionally, the EDP profiles for all archetypes are also provided as supplementary material [20].

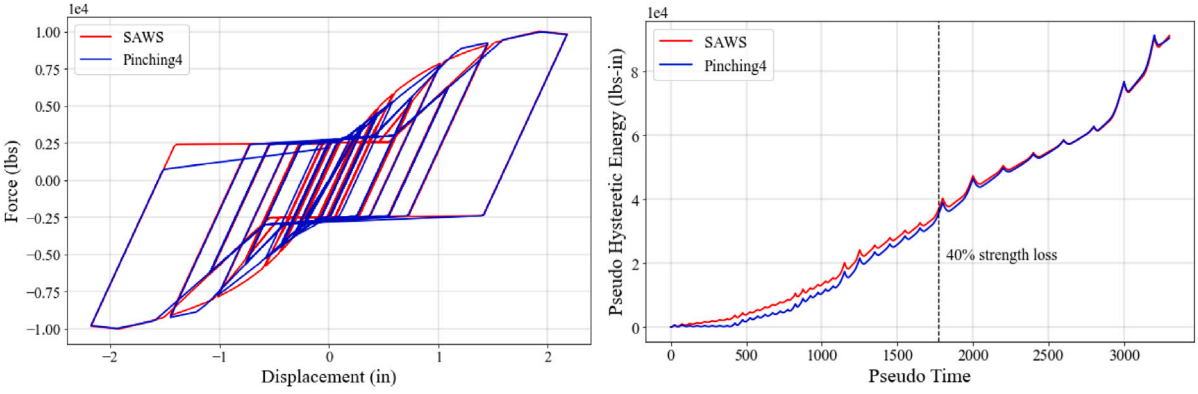

Fig. 2. (a) Comparison of the cyclic force–displacement behavior computed using the SAWS (CASHEW) and Pinching4 (OpenSEES) hysteretic models; (b) pseudo energy plots based on the dissipated energy.

Table 2
Comparison of eigenvalue and pushover analysis results between FEMA P-2139-2 and the current study.

Archetype ID	Fundamental period (sec)		Base strength (V_{max}/W)		Drift @ 80% V_{max}/W(%)		Ductility demand
	FEMA P-2139	OpenSees	FEMA P-2139	OpenSees	FEMA P-2139	OpenSees	
SFD1B	0.14	0.13	2.10	2.28	3	3.54	0.22
SFD3B	0.13	0.13	2.33	2.53	3	3.52	0.16
SFD2B	0.24	0.22	0.90	1.04	2	1.89	0.26
SFD4B	0.24	0.22	0.95	1.14	2	1.94	0.28
MFD1B	0.18	0.16	1.39	1.51	3	3.08	0.99
MFD4B	0.18	0.16	1.48	1.75	3	3.51	0.69
MFD2B	0.27	0.26	0.70	0.67	1	1.99	1.22
MFD5B	0.27	0.26	0.73	0.72	2	2.21	1.14
MFD3B	0.51	0.49	0.39	0.39	1	1.31	2.28
MFD6B	0.54	0.49	0.44	0.48	1	1.41	1.74

5. Case studies

This section provides a detailed comparative analysis of the various IM evaluation methods described in Section 2. The analysis is performed at two levels of granularity. In the first part, the pros and cons of each method are discussed based on the EDP data from an individual building. In the second half, results from all 10 archetypes are aggregated and discussed.

5.1. IM evaluation for a single building

For an in-depth IM evaluation, the four-story MFD (archetype ID: MFD6B) is chosen. The bi-directional (X- and Z-axis) SDR and PFA profiles are leveraged to investigate the effectiveness of the 10 IMs considered.

5.1.1. Investigating the multivariate distribution assumption

The methods detailed in Section 2 rely on foundational assumptions that the EDPs, IMs, and causal parameters can be modeled by univariate or multivariate distributions that can be defined by a fixed set of parameters. The first step in implementing the outlined methods is validating or equivalently quantifying the degree of invalidity of the parametric assumptions. This ensures that the probability models are not misspecified. If they are misspecified, the uncertainty propagated due to an invalid assumption should be quantified to make accurate inferences [47]. For the majority of this study, EDPs, IMs, and causal parameters are assumed to follow a multivariate lognormal distribution. In statistics, normality tests such as the Kolmogorov–Smirnov test and Shapiro–Wilk test are widely used to evaluate this type of hypothesis. However, previous authors have noted that normality tests for large datasets might be irrelevant [48]. Specifically, the authors argued that for a moderately large enough dataset ($n > 40$), the violation of normality would not cause major problems. Conceptually, it is trivial that for a large sample size, even the slightest deviation from normality will result in failed normality tests. Considering that the EDPs, IMs, and causal parameters have some degree of randomness, they are not empirically expected to follow a perfectly multivariate lognormal relationship. This can be rationalized by using as a measure the Kullback–Leibler divergence between the two closest Gaussian distributions to the actual distributions, rather than the distributions themselves. Rather, it is appropriate to gauge the relative measure of dependence between multiple random variables in terms of mutual information. Mutual information is a measure of information obtained about one random variable by observing the other. Mutual information between two random variables, X and Y, is computed as

$$I(X;Y) = D_{\mathrm{KL}}\left(P_{X,Y} \parallel P_X \otimes P_Y\right) = \int_Y \int_X P_{X,Y}(x,y) \log\left(\frac{P_{X,Y}(x,y)}{P_X(x)P_Y(y)}\right) dx dy \quad (12)$$

As noted in Eq. (12), mutual information relies on KL divergence to determine how much the joint distribution ($P_{X,Y}$) differs from the product of two marginal distributions (P_X and P_Y). When the joint distribution coincides with the product of the marginals, the mutual information equals zero, thus, effectively indicating that the two random variables are independent. It also implies that observing X provides no information about Y. Mutual information is a non-negative number and is symmetric (i.e., $I(X;Y) = I(Y;X)$). Fig. 3 presents a heat map of mutual information between SDR_X and PFA_X at story 1 of MFD6B, Sa_{T1}, M, and R. The non-zero mutual information across the board implies the existence of dependence between the respective pairs. The mutual information, however, cannot be easily interpreted solely based on its value because it is not a standardized quantity like the correlation coefficient. To infer a sense of the degree of dependence,

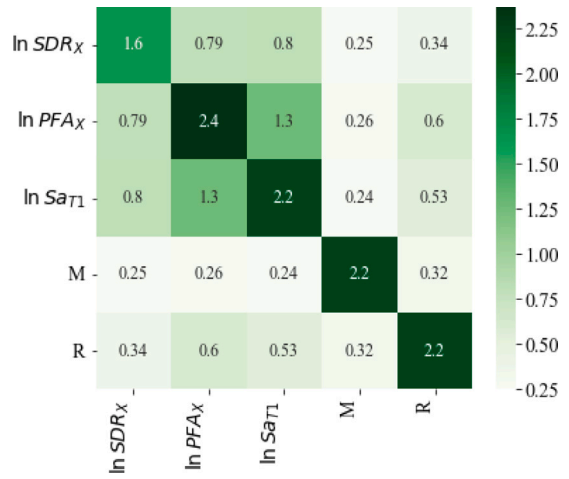

Fig. 3. Mutual Information between SDR and PFA at floor 1 in X-direction, Sa_{T1}, magnitude, and distance.

self-information can be used as a baseline reference point. In a special case where the two random variables follow a bivariate normal distribution, mutual information has a closed-form relationship to the correlation coefficient (ρ), i.e. $I(X,Y) = -\frac{1}{2}log(1-\rho^2)$. A random variable would be perfectly correlated ($\rho = 1.0$) to itself, but for the purposes of computation, we will assume a near-perfect correlation $\rho = 0.999$ because $\log(0)$ is undefined. The self-information between two perfectly correlated random variables equals 3.10 bits. In Fig. 3, the diagonal terms are expected to be close to 3.10 bits. The off-diagonal terms can be compared to their respective diagonal term to gauge the degree of joint relationship. As expected, log-transformed SDR_X, PFA_X, and Sa_{T1} share the highest information. Among the causal parameters, mutual information for R is roughly double compared to M suggesting that R has relatively stronger mutual dependence with SDR_X, PFA_X, and Sa_{T1}. It is noted that the conclusion drawn here is valid for the specific set of considered ground motions and the findings may vary if the record-set is changed.

5.1.2. Efficiency comparisons

Fig. 4 shows the story-based efficiency profile of all 10 IMs for the four-story building (MFD6B). Although the figure represents efficiency profiles, it is obtained by implementing the traditional OLS method. In other words, the direction-dependent EDPs are individually regressed on all the IMs. For 16 EDPs (8 SDRs and 8 PFAs) and 10 IMs, the RSEs obtained from 160 OLS are represented in the plot.

The efficiency profiles for SDR and PFA are nearly symmetrical in the X- and Z-direction. This is indicative of a similar wall density along the X- and Z-direction. For SDR, the dispersion profile along the story height suggests Sa_{avg} and Sa_{T1} to be the most efficient IMs. In predicting PFA along the X-direction, all the acceleration-based IMs showcase similar predictive ability with Sa_{avg} performing slightly better on average over the height. However, in the Z-direction, the dispersion is constant over the height and ASI is distinctly the most efficient IM followed by PGA. It is interesting to note that acceleration, velocity, and displacement-based intensity measures are roughly grouped together with the same dispersion profile and progressively higher dispersion values.

Based on the discussion above, it is challenging to pinpoint a single "most efficient" IM for all the EDPs. Of course, one could take the average of dispersions, or only consider the maximum EDP instead of the profile to summarize the results but these approaches have two shortcomings (1) the summarized data will potentially lose some information, and (2) it would not be able to account for mutual dependence. Fig. 5 compares the entropy for each IM obtained by implementing a multivariate GAM model that incorporates all 16 EDPs. When the nonlinear and multivariate relationship is explicitly modeled, ASI is the most efficient IM. ASI was introduced to study short-period structures such as dams. It is therefore not surprising that it has the least uncertainty in estimating the seismic demands of a four-story building with a first-mode period of 0.49 s. Appropriately, Sa_{avg} is more efficient than Sa_{T1} because Sa_{avg} naturally contains more information than an elastic spectral intensity (Sa_{T1}). Similar to Fig. 4, it is apparent in Fig. 5 that acceleration-based IMs are relatively more efficient than velocity- and displacement-based IMs.

5.1.3. Sufficiency comparisons

As detailed in Section 2.2, sufficiency can be characterized using either a p-value or relative entropy. This section provides a detailed implementation of univariate and multivariate cases for both the traditional OLS-based and entropy-based methods. Table 3 summarizes the p-values obtained by regressing the residuals ($\ln(\epsilon|\text{IM})$) independently against the causal parameters per Eq. (5). In total, 32 univariate OLS models and two 16-dimensional multivariate GAM models are fitted for each IM of interest. To limit the number of models, Table 3 only documents the results for SDR and PFA in the X-direction on the fourth floor. The p-values for the majority of causal parameter and IM pairs are well below the 5% threshold, indicating that most of the IMs are not sufficient in defining the structural response. For both OLS and GAM, it can be argued that PGA is the most sufficient IM.

To better summarize a large number of possible p-values in significance testing, a sufficiency rate is introduced as an aggregate measure. The sufficiency rate is defined as the fraction of sufficient cases within all EDPs against a specific causal parameter. For instance, in Table 3, Sa_{T1} is sufficient with respect to R in one out of the two possible OLS models. In this case, the sufficiency rate is 50%. Similarly, the sufficiency rate for the GAM model is 0% because Sa_{T1} is not sufficient against any causal parameters. Table 4 lists the sufficiency rates for all 10 IMs. For the univariate OLS, Sa_{T1} is the most sufficient with respect to M while PGA is the most sufficient for R. On aggregate, PGA appears to be the most sufficient IM considering all causal parameters, Similarly, for the multivariate GAM (Eq. (6), PGV is the most sufficient with respect to M while Sa_{avg} is the most sufficient for R. On average, PGV is the most sufficient IM. As noted earlier, the multivariate GAM can be modified to consider two-way or three-way interactions between the IM and causal parameters (i.e., Eq. (7)). In Table 4, only the sufficiency rate from a two-way interaction GAM (Eq. (7a)) is presented because the sufficiency rate for three-way interactions (Eq. (7b)) is zero for all cases. The multivariate GAM has a higher overall sufficiency rate for velocity-based IMs as compared to the OLS-based approach. This could be because the GAM is designed to account for nonlinear relationships through the spline function. The alternate GAM, on the other hand, has higher sufficiency for acceleration-based IMs and is exclusively sufficient against R. This implies that the two-way interaction between IM and M is more significant than IM and R.

As highlighted in Table 3, PGA is considered marginally sufficient (p-value = 0.0467) against M when the GAM model is implemented. Although, given that the p-value is less than 5%, it can also be argued that PGA is marginally insufficient. The judgment would rely on the researcher's choice of the level of significance (α). Table 5 compares the KL divergence (relative entropy) for the univariate and multivariate cases. In the univariate case, P is the distribution of the EDP conditioned on the IM in the form of residuals ($\ln(\epsilon|\text{IM})$) while Q is the distribution of the EDP conditioned on the IM and a causal parameter x (either M or R) in the form of residuals (i.e., $\ln(\epsilon|\text{IM}, x)$. Concurrently, $\mathcal{N}_0$ and $\mathcal{N}_1$ are the jointly normal distribution of maximum SDR and PFA with and without a causal parameter, respectively. For simplification, all KL divergence calculations hereafter utilize the maximum EDPs in each direction instead of the EDP profile. In the univariate relative entropy, KL divergence for SDR and PFA are added to make an equivalent comparison with its multivariate counterpart.

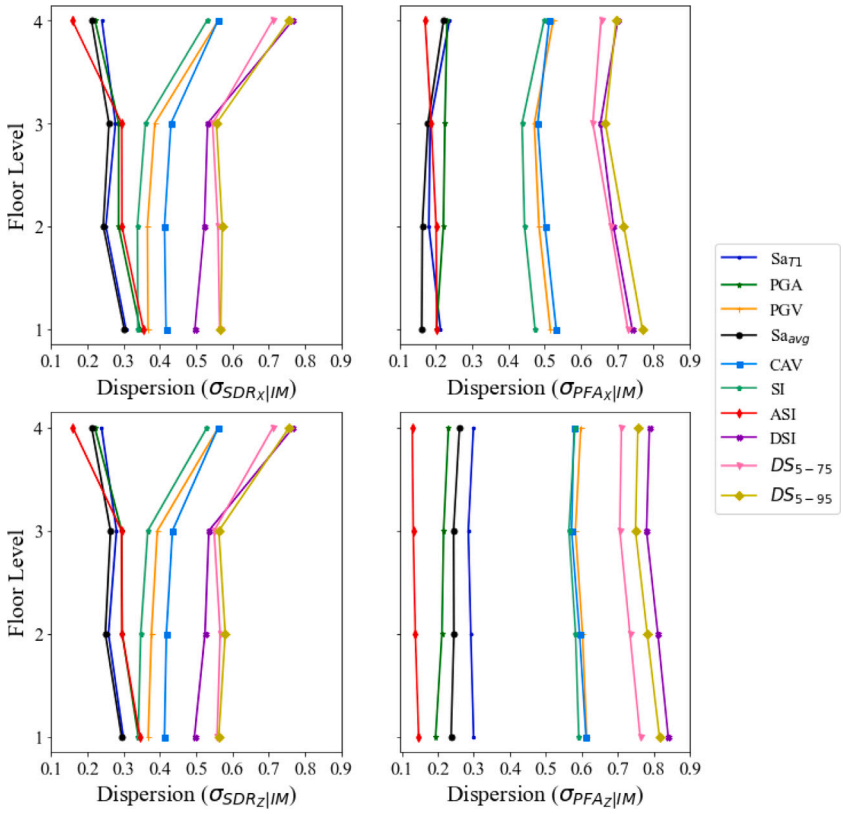

Fig. 4. Story-level efficiency ($\sigma_{EDP|IM}$) of SDR and PFA of a four-story multi-family building (MFD6B).

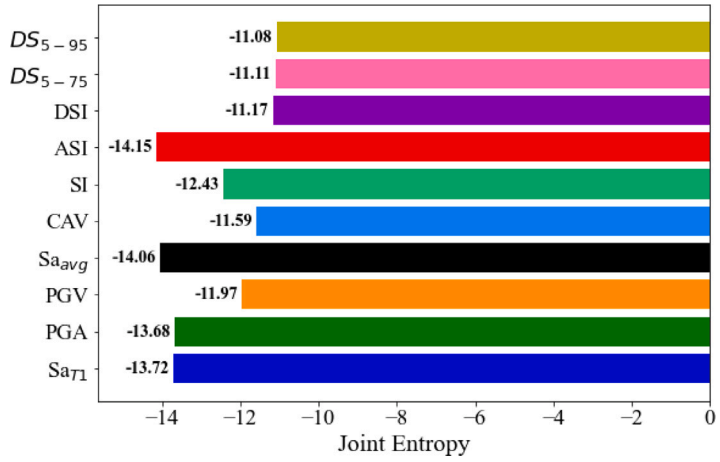

Fig. 5. Multivariate entropy-based efficiency for the four-story multi-family building (MFD6B).

Table 3
Comparison of *p*-values obtained from univariate OLS and multivariate GAM models. The residuals, $\ln(\epsilon|IM)$, are regressed on the causal parameters (M and R) independently.

IM type	OLS: SDR		GAM: SDR		OLS: PFA		GAM: PFA	
	Against M	Against R	Against M	Against R	Against M	Against R	Against M	Against R
Sa_{T1}	<0.0001	<0.0001	<0.0001	<0.0001	<0.0001	**0.69**	<0.0001	<0.0001
PGA	**0.89**	**0.86**	**0.05**	0.008	**0.17**	<0.0001	**0.59**	**0.17**
PGV	<0.0001	<0.0001	<0.0001	<0.0001	<0.0001	<0.0001	<0.0001	<0.0001
Sa_{avg}	<0.0001	**0.34**	<0.0001	<0.0001	<0.0001	<0.0001	<0.0001	<0.0001
CAV	<0.0001	<0.0001	<0.0001	<0.0001	<0.0001	<0.0001	<0.0001	<0.0001
SI	<0.0001	<0.0001	<0.0001	<0.0001	<0.0001	<0.0001	<0.0001	<0.0001
ASI	<0.0001	**0.10**	<0.0001	<0.0001	<0.0001	<0.0001	<0.0001	0.04
DSI	<0.0001	<0.0001	<0.0001	<0.0001	<0.0001	<0.0001	<0.0001	<0.0001
DS_{5-75}	<0.0001	<0.0001	<0.0001	<0.0001	<0.0001	<0.0001	<0.0001	<0.0001
DS_{5-95}	<0.0001	<0.0001	<0.0001	<0.0001	<0.0001	<0.0001	<0.0001	<0.0001

Table 4
Sufficiency rate (%) based on the number of sufficiency cases for OLS and GAM-based sufficiency checks. The sufficiency rate for the multivariate GAM is computed using Eq. (6) while the alternate GAM is computed using Eq. (7a).

IM type	Univariate OLS			Multivariate GAM- Eq. (6)			Alternate GAM- Eq. (7a)		
	Against M	Against R	Overall	Against M	Against R	Overall	Against M	Against R	Overall
Sa_{T1}	**31.25**	12.5	21.88	12.5	0	6.25	0	0	0
PGA	25	**43.75**	**34.38**	12.5	37.5	25	0	37.5	18.75
PGV	0	0	0	**93.75**	0	**43.75**	0	0	0
Sa_{avg}	18.75	37.5	28.22	12.5	**43.75**	28.13	0	**56.25**	**28.13**
CAV	0	0	0	18.75	0	9.38	0	0	0
SI	0	0	0	81.25	0	40.63	0	0	0
ASI	25	37.5	31.25	18.75	18.75	18.75	0	18.75	9.38
DSI	0	0	0	0	0	0	0	0	0
$DS_{5\text{-}75}$	0	0	0	0	0	0	0	0	0
$DS_{5\text{-}95}$	0	0	0	0	0	0	0	0	0

Table 5
The univariate relative entropy computed based on residuals from the OLS and the multivariate relative entropy computed based on estimated residuals from the GAM model. The relative entropy is the measure of relative sufficiency. The KL divergence values are scaled by a factor of 1×10^3.

IM type	Univariate Entropy $D_{KL}(P \parallel Q)$			Multivariate Entropy $D_{KL}(\mathcal{N}_0 \parallel \mathcal{N}_1)$		
	Including M	Including R	Total	Including M	Including R	Total
Sa_{T1}	1.58	4.54	6.12	2.88	6.64	9.53
PGA	2.29	3.53	5.81	2.66	4.99	7.65
PGV	5.18	19.9	25.1	6.05	19.7	25.7
Sa_{avg}	2.77	**1.81**	**4.58**	4.00	**2.02**	**6.01**
CAV	31.4	90.3	121	31.8	95.18	127
SI	2.40	13.2	15.6	3.30	13.9	17.3
ASI	3.64	5.04	8.68	3.84	6.68	10.5
DSI	**0.47**	150	150	**1.45**	118	119
$DS_{5\text{-}75}$	33.8	199	233	23.9	149	173
$DS_{5\text{-}95}$	16.4	203	220	13.1	152	166

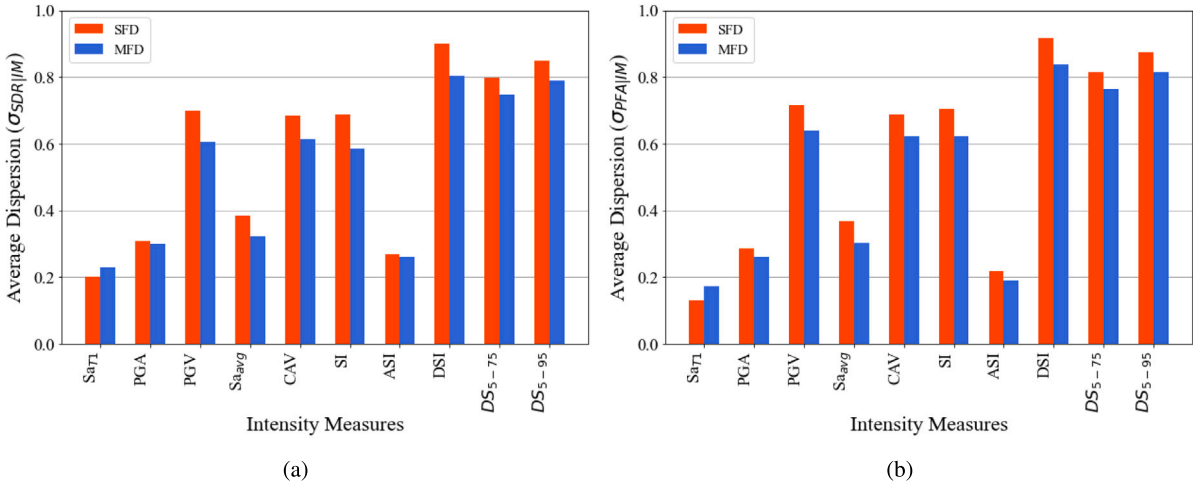

Fig. 6. Average efficiency of (a) SDR ($\sigma_{SDR|IM}$) and (b) PFA ($\sigma_{PFA|IM}$) among four SFDs (red) and six MFDs (blue) for all 10 IMs considered.

It can be seen that Sa_{avg} typically has the lowest KL divergence implying that, relatively speaking, it is the most sufficient IM. The four-story residential building used in this example is known to have nonlinear behavior controlled by multiple modes [39]. It is not surprising that Sa_{avg}, which encompasses spectral acceleration information for a range of periods is the most sufficient in rendering the conditional distribution of EDP independent of the causal parameters. Several past studies have found Sa_{avg} to be sufficient for structures known to undergo highly nonlinear behavior under dynamic loading [9,13].

5.2. IM evaluation for the complete archetype set

The efficiency and sufficiency results for the 10 archetype woodframe buildings are summarized in this section.

5.2.1. Efficiency summary

OLS-based efficiency. For the set of 10 archetype woodframe buildings, the OLS-based dispersion is averaged at two stages. First, the average dispersion is computed for an individual building (considering all stories/floor levels and directions) which is then averaged among all the relevant buildings. Fig. 6(a) shows that Sa_{T1} is the most efficient IM in estimating SDR because it has the lowest average dispersion among both the SFD and MFD buildings. In Fig. 6(b), a near identical trend was observed for PFA where Sa_{T1} was found to be the most efficient followed by Sa_{avg}. It is apparent from Fig. 6 that acceleration-based IMs (Sa_{T1}, PGA, Sa_{avg}, and ASI), velocity-based IMs (PGV, CAV, SI), and displacement-based IMs (DSI, $DS_{5\text{-}75}$, and $DS_{5\text{-}95}$) cluster together and tend to have progressively higher average dispersion across the building groups. Recall that a similar pattern was also observed in

Table 6
Total KL divergence (relative entropy) among EDPs and across causal parameters computed assuming the univariate relationship between EDPs. The KL divergence values are scaled by a factor of 1×10^3.

Archetype ID	Period (T_1)	Sa_{T1}	PGA	PGV	Sa_{avg}	CAV	SI	ASI	DSI	$DS_{5\text{-}75}$	$DS_{5\text{-}95}$
SFD1B	0.13	**3.80**	10.9	85.0	34.5	309	61.9	6.26	276	225	235
SFD3B	0.13	**2.45**	10.7	86.6	34.5	319	62.8	5.81	280	234	243
MFD1B	0.16	**8.25**	9.44	94.3	30.2	302	72.1	8.30	298	235	245
MFD4B	0.16	11.9	**10.9**	103	31.9	314	80.1	11.1	318	252	263
SFD2B	0.22	15.5	**7.85**	90.3	25.0	282	70.1	11.3	294	241	250
SFD4B	0.22	25.9	**16.0**	107	30.2	294	87.6	21.4	333	280	290
MFD2B	0.26	31.6	**14.2**	95.5	23.6	293	74.5	21.4	319	300	305
MFD5B	0.26	11.7	**5.50**	56.4	11.2	207	43.3	7.23	236	252	257
MFD3B	0.49	21.4	14.9	44.8	**12.8**	183	31.4	21.6	211	290	279
MFD6B	0.49	6.13	5.81	25.0	**4.58**	122	15.6	8.68	150	233	220

Table 7
Total KL divergence (relative entropy) among EDPs and across causal parameters computed assuming the multivariate relationship between EDPs. The KL divergence values are scaled by a factor of 1×10^3.

Archetype ID	Period (T_1)	Sa_{T1}	PGA	PGV	Sa_{avg}	CAV	SI	ASI	DSI	$DS_{5\text{-}75}$	$DS_{5\text{-}95}$
SFD1B	0.13	**6.35**	10.9	62.0	24.8	183	49.8	8.14	179	141	145
SFD3B	0.13	**4.15**	9.75	57.7	23.0	182	45.3	6.55	169	141	144
MFD1B	0.16	**8.70**	10.3	66.1	25.3	186	54.6	9.88	193	147	151
MFD4B	0.16	**12.4**	12.8	73.0	29.0	201	60.8	12.9	208	163	167
SFD2B	0.22	18.4	**13.2**	76.8	27.6	209	62.8	16.7	226	186	189
SFD4B	0.22	26.4	**19.8**	87.1	33.4	232	73.2	23.9	247	216	219
MFD2B	0.26	32.2	**17.1**	79.8	27.0	234	63.8	22.3	240	231	230
MFD5B	0.26	12.6	**7.39**	43.8	11.5	167	34.2	8.30	160	179	180
MFD3B	0.49	27.8	17.8	47.1	**13.5**	191	35.2	25.8	178	238	228
MFD6B	0.49	9.53	7.65	25.7	**6.01**	127	17.3	10.5	119	173	166

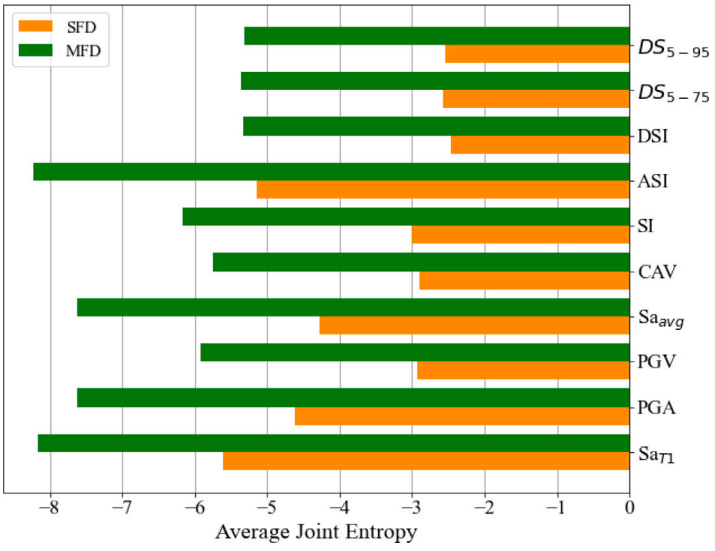

Fig. 7. Average joint entropy of SDR and PFA ($\sigma_{SDR,PFA|IM}$) among four SFDs (orange) and six MFDs (green) for all the IMs.

the individual building assessment discussed in Section 5.1.2. It is also notable that the average dispersion for Sa_{T1}, PGA, and ASI, is lower in predicting PFA as compared to SDR. On the other hand, the dispersion of the velocity- and displacement-based IMs is higher in PFA than SDR.

Joint entropy-based efficiency. Fig. 7 displays the average joint entropy across the four SFDs (in orange) and six MFDs (in green) for each of the 10 IMs. For both categories of buildings, acceleration-based IMs such as Sa_{T1}, PGA, Sa_{avg}, and ASI outperform velocity- and displacement-based IMs. Evidently, Sa_{T1} is the most efficient IM among SFDs while ASI edges Sa_{T1} by a slight margin to be the most efficient for the MFDs. This observation conforms to the expected structural behavior of the archetypes. Meaning, it is reasonable for an elastic, period-dependent Sa_{T1} to be efficient for highly ductile SFDs that are not expected to collapse for a relatively large displacement. MFDs, on the other hand, are moderately ductile and tend to have multi-modal inelastic responses. Thus, it is plausible to observe ASI, which is an aggregate of Sa_{T1} from 0.1 to 0.5 s, to be the most efficient as compared to Sa_{T1} and other IMs. This pattern indicates that when the EDPs are assumed to be multivariate, more complex IMs such as ASI perform better in defining the demand model for buildings dominated by multiple modes. Recall that the univariate OLS-based method (Fig. 6) established Sa_{T1} to be the most efficient for all 10 buildings regardless of the level of ductility of the building. Interestingly, the trend across different IMs for SFD and MFD is identical irrespective of the univariate or multivariate assumption. This implies that both the univariate and multivariate approaches can distinguish the performance of different IMs. This comparison also suggests that additional studies are needed (especially for other types of lateral force resisting systems) to further investigate the implications of the univariate versus multivariate assumption.

5.2.2. Sufficiency summary

As highlighted in Section 2.2, there are various methods for determining if the distribution of an EDP conditioned on the IM is

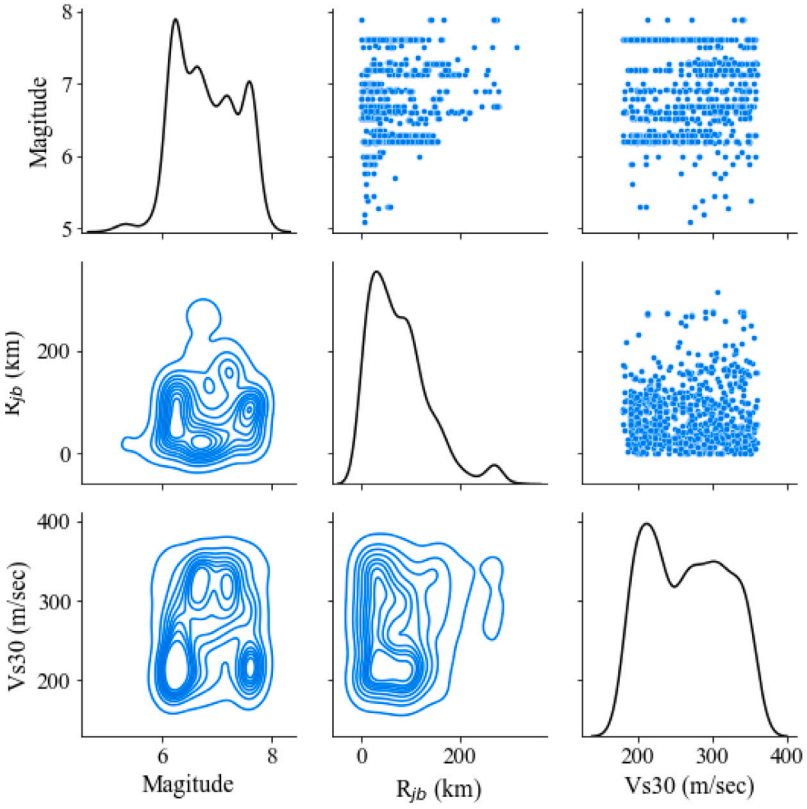

(a)

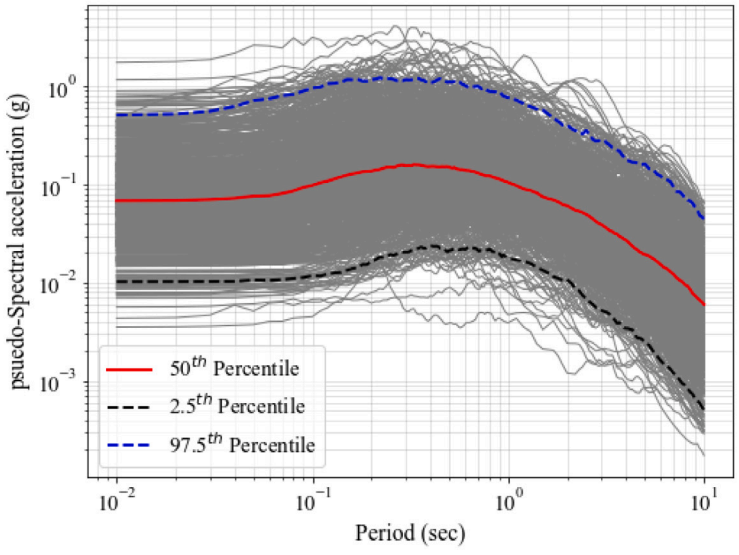

(b)

Fig. 8. (a) A three-way grid plot showing individual (diagonal) and pairwise (off-diagonals) relationships between three causal parameters, magnitude, distance (R_{jb}), and shear-wave velocity (Vs_{30}). (b) Rotated response spectrum (RotD50) of all 826 ground motion pairs (in gray) and the median of all the records (in red).

independent of the causal parameters. The merits of each method have been previously discussed at length. For the complete archetype set assessment, univariate and multivariate relative entropy-based methods are presented.

Univariate relative entropy. Table 6 summarizes the KL divergence between the univariate conditional EDP distribution with and without causal parameters. Each value is the sum of KL divergence between all the causal parameters and EDPs. For instance, the values for MFD6B are the same as the total value presented in Table 5. The least relative entropy in each row is highlighted in bold font thus indicating the most sufficient IM. It is seen that the sufficiency trend is a function of the building's fundamental period and/or the displacement ductility demand. Sa_{T1} is sufficient for one-story buildings while PGA is sufficient for two-story buildings. In both the one- and two-story

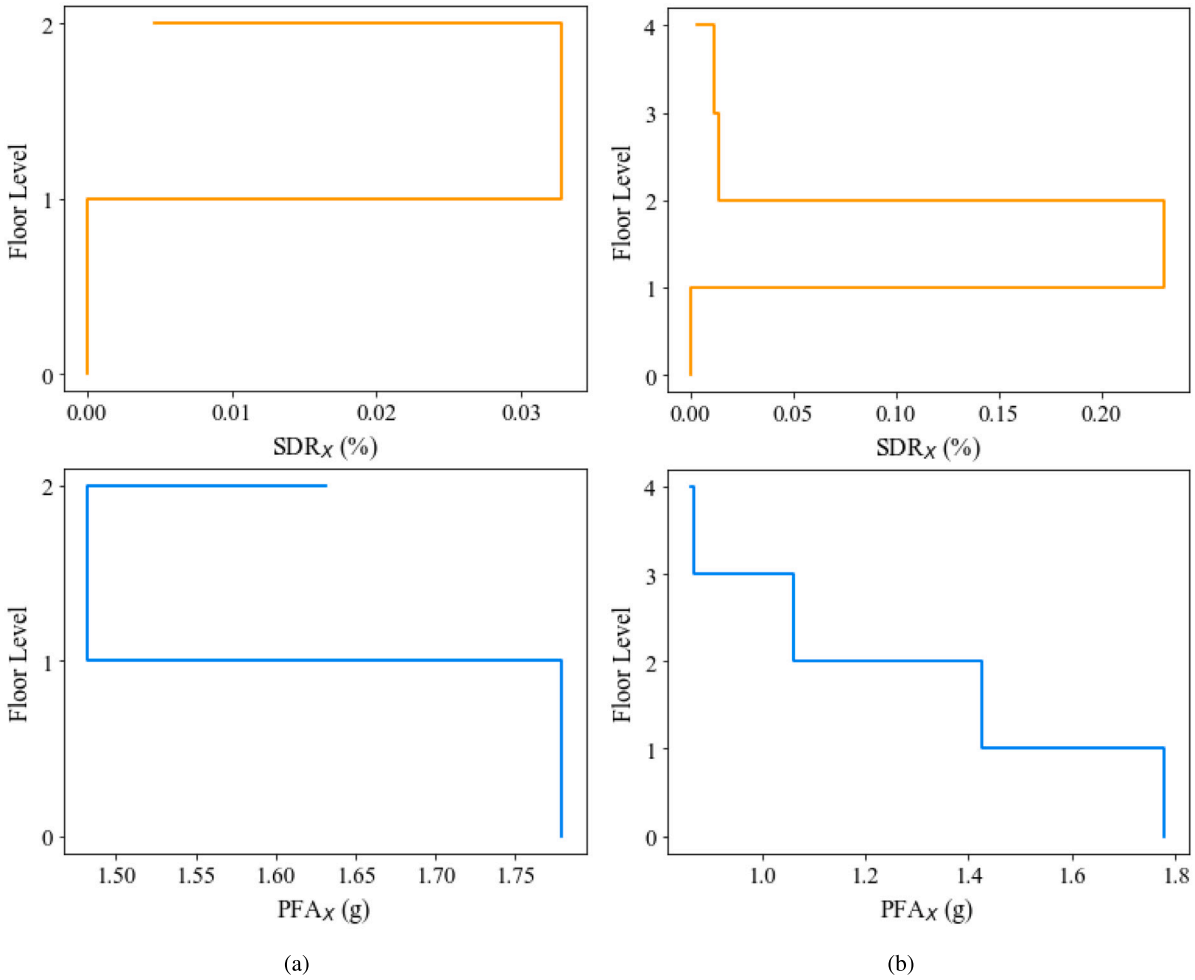

Fig. 9. (a) EDP profile of a two-story archetype (SFD2B) and (b) EDP profile of a four-story archetype (MFD3B).

buildings, ASI is the second most sufficient IM. The one- and two-story buildings have first-mode fundamental periods less than 0.26 s and an average displacement ductility demand of 0.62. To this end, it is logical that IMs such as Sa_{T1}, PGA, and ASI are sufficient in general. However, for the four-story buildings that undergo highly nonlinear behavior and are also subjected to higher mode responses, Sa_{avg} is the most sufficient IM. Among the archetypes, the four-story buildings (on average) have a ductility demand of 2.01 which indicates that they experience the much higher inelastic deformations compared to their one- and two-story counterparts. This result highlights the ability of Sa_{avg} to capture ground motion effects on a structure that responds to a range of frequencies due to period elongation and/or higher mode effects.

Multivariate relative entropy. Table 7 shows the KL divergence when the max SDR and PFA are assumed to follow a bivariate lognormal distribution. Each value represents the total KL divergence for all causal parameters. For instance, the values for archetype MFD6B are the same as the total value previously presented in Table 5. The sufficiency trend is more distinct as compared to Table 6. Under the bivariate assumption, Sa_{T1}, PGA, and ASI appear to be the most sufficient for the one-story and two-story buildings while Sa_{avg} is the most sufficient for the four-story buildings.

6. Conclusions

This paper presented a comparative assessment of alternative methods for evaluating and selecting the most appropriate ground motion intensity measure (IM) for nonlinear response history analyses. Specifically, efficiency and sufficiency are discussed as the two primary evaluation metrics. Historically, univariate linear regression (OLS) has been used for both types of evaluations, which disregards the nonlinear multivariate relationships between the engineering demand parameters (EDPs), IMs, and causal parameters. Recently, entropy-based measures have been proposed that address the limitations of the OLS-based methods but the relevant studies still relied on the univariate assumption.

In this study, the currently available univariate OLS-based methods are expanded to explicitly consider the multivariate distribution of EDPs. In particular, a multi-target generalized additive model (GAM) is proposed as an alternative to the OLS approach. The GAM appropriately captures the complex relationship within a given EDP (i.e., the response along the building height in the two orthogonal directions), between EDPs (e.g., story drift ratio (SDR) and peak floor acceleration (PFA)), and between the IM and EDPs. The GAM is implemented to compute the joint entropy as an alternative measure of efficiency and the p-value of the spline function as a measure of sufficiency. The EDP data generated from 10 woodframe buildings using a site-agnostic set of 826 pairs of ground motion records is leveraged to evaluate 10 different IMs. The results from both the univariate OLS and multivariate GAM suggest that Sa_{T1} and acceleration spectrum intensity (ASI) are the most efficient IMs across all building types. Also, for all IMs, greater efficiency was obtained for the single-family dwellings (SFDs) compared to the multi-family residences. The higher ductility demands in the multi-family dwellings (MFDs) was used to explain this result.

A comparative analysis between the existing and proposed relative entropy-based sufficiency methods is also performed using the set of aforementioned building archetypes and IMs. In the univariate case, Sa_{T1} appeared to be the most sufficient for all but one of the 1-story buildings, whereas, peak ground acceleration (PGA) and Sa_{avg} were found to be the most sufficient for the 2- and 4-story buildings, respectively. In the multivariate case, the sufficiency trend was even more distinguished such that Sa_{T1} was found to be the most sufficient for all 1-story buildings, PGA the most sufficient for all 2-story buildings, and Sa_{avg} the most sufficient for all four-story buildings. Overall, it is seen that Sa_{avg} is sufficient for structures that respond to a range of frequencies whereas Sa_{T1}, PGA, and ASI are sufficient for shorter buildings with a fundamental period less than 0.26 s.

The results from this study suggest that capturing the multivariate EDP distribution in IM evaluations has non-negligible implications, especially for multi-story woodframe buildings. However, both the univariate and multivariate methods demonstrated that a single universally optimal IM likely does not exist for a set of building archetypes. Rather, there was clear evidence that the efficacy of an IM is a function of the level of nonlinearity (or ductility demand) in the response of the structure. To facilitate future applications of the various evaluation methods, the source code developed as a part of this research work is made publicly available in a GitHub Repository [20]. The repository includes code for the GAM- and univariate OLS-based approaches.

While the alternative methods presented thus far are sound approaches to evaluating the effectiveness of an IM, there are several limitations. Ground motion models often utilize a host of causal parameters such as soil type, fault type, and shear-wave velocity, which were not considered in this study. There is an opportunity for future IM evaluation studies to investigate these often-ignored causal parameters. The current study used a suite of unscaled ground motion records to negate the possibility of bias being induced due to amplitude scaling. However, it is noted that the use of unscaled records comes with its own challenges as the two extreme ends of the IM distribution could be dominated by a very specific set of causal parameters (low M and large R in low-intensity IMs, and high M and low R in high-intensity IMs). Finally, most of the alternative methods rely on the assumption that the EDPs, IMs and causal parameters for a theoretical multivariate distribution (usually lognormal) that should be further investigated for different classes of structures.

Declaration of competing interest

The authors declare that they have no known competing financial interests or personal relationships that could have appeared to influence the work reported in this paper.

Data availability

Link to the Github page is included in the paper.

Acknowledgments

The authors would like to acknowledge Pablo Heresi and Eduardo Miranda for sharing the ground motion records information. We would also like to thank two anonymous reviewers for their comments which helped advance the quality of this paper.

Appendix A. Ground motion information

See Fig. 8.

Appendix B. Engineering demand parameters

Fig. 9 highlights the EDP profiles along the building height for a two-story single-family dwelling (Fig. 9(a)) and a four-story multi-family dwelling (Fig. 9(b)). The figures show the peak story drift ratio and peak floor acceleration in the X-direction experienced by the archetypes when subjected to 826 pairs of ground motion records. It can be seen that the four-story archetype experiences higher story drift ratio as compared to its two-story counterpart.

References

[1] FEMA. Seismic performance assessment of buildings. FEMA P-58, vol. 1- methodology, 2nd ed.. Washington, D.C.: Federal Emergency Management Agency; 2012.
[2] Luco N, Cornell CA. Structure-specific scalar intensity measures for near-source and ordinary earthquake ground motions. Earthq Spectra 2007;23(2):357–92.
[3] Campbell KW, Bozorgnia Y. NGA-West2 ground motion model for the average horizontal components of PGA, PGV, and 5% damped linear acceleration response spectra. Earthq Spectra 2014;30(3):1087–115.
[4] Shome N, Cornell CA, Bazzurro P, Carballo JE. Earthquakes, records, and nonlinear responses. Earthq Spectra 1998;14(3):469–500.
[5] Bradley BA, Dhakal RP, MacRae GA, Cubrinovski M. Prediction of spatially distributed seismic demands in specific structures: Ground motion and structural response. Earthq Eng Struct Dynam 2010;39(5):501–20.
[6] Padgett JE, Nielson BG, DesRoches R. Selection of optimal intensity measures in probabilistic seismic demand models of highway bridge portfolios. Earthq Eng Struct Dynam 2008;37(5):711–25.
[7] Baker JW, Allin Cornell C. A vector-valued ground motion intensity measure consisting of spectral acceleration and epsilon. Earthq Eng Struct Dynam 2005;34(10):1193–217.
[8] Aslani H. Probabilistic earthquake loss estimation and loss disaggregation in buildings. Stanford University; 2005.
[9] Eads L, Miranda E, Lignos DG. Average spectral acceleration as an intensity measure for collapse risk assessment. Earthq Eng Struct Dynam 2015;44(12):2057–73.
[10] Kohrangi M, Vamvatsikos D, Bazzurro P. Implications of IM selection for seismic loss assessment of 3D buildings. Earthq Spectra 2016;32(4):2167–89. http://dx.doi.org/10.1193/112215EQS177M.
[11] Kazantzi AK, Vamvatsikos D. Intensity measure selection for vulnerability studies of building classes. Earthq Eng Struct Dynam 2015;44(15):2677–94.
[12] Dhulipala SL, Rodriguez-Marek A, Ranganathan S, Flint MM. A site-consistent method to quantify sufficiency of alternative IMs in relation to PSDA. Earthq Eng Struct Dynam 2018;47(2):377–96.
[13] Du A, Padgett JE. Entropy-based intensity measure selection for site-specific probabilistic seismic risk assessment. Earthq Eng Struct Dynam 2021;50(2):560–79.
[14] Hastie TJ, Tibshirani RJ. Generalized additive models. Routledge; 2017.
[15] Jalayer F, Beck J, Zareian F. Analyzing the sufficiency of alternative scalar and vector intensity measures of ground shaking based on information theory. J Eng Mech 2012;138(3):307–16.
[16] Heresi P, Miranda E. Intensity measures for regional seismic risk assessment of low-rise wood-frame residential construction. J Struct Eng 2021;147(1):04020287.
[17] Shome N. Probabilistic seismic demand analysis of nonlinear structures. Stanford University; 1999.
[18] Aslani H, Miranda E. Probability-based seismic response analysis. Eng Struct 2005;27(8):1151–63.
[19] Friedman JH, Stuetzle W. Projection pursuit regression. J Amer Statist Assoc 1981;76(376):817–23.
[20] Dahal L. Alternative methods for evaluating the optimality of ground motion intensity measure. 2022, GitHub Repository, GitHub, https://github.com/laxmandahal/IM_Study.
[21] Ancheta TD, Darragh RB, Stewart JP, Seyhan E, Silva WJ, Chiou BS-J, et al. NGA-West2 database. Earthq Spectra 2014;30(3):989–1005.
[22] Heresi P, Dávalos H, Miranda E. Ground motion prediction model for the peak inelastic displacement of single-degree-of-freedom bilinear systems. Earthq Spectra 2018;34(3):1177–99.
[23] Luco N, Bazzurro P. Does amplitude scaling of ground motion records result in biased nonlinear structural drift responses? Earthq Eng Struct Dynam 2007;36(13):1813–35.
[24] Dávalos H, Miranda E. Evaluation of bias on the probability of collapse from amplitude scaling using spectral-shape-matched records. Earthq Eng Struct Dynam 2019;48(8):970–86.
[25] Tsalouchidis KT, Adam C. Amplitude scaling of ground motions as a potential source of bias: Large-scale investigations on structural drifts. Earthq Eng Struct Dynam 2022;51(12):2904–24.

[26] Bojórquez E, Chávez R, Reyes-Salazar A, Ruiz SE, Bojórquez J. A new ground motion intensity measure IB. Soil Dyn Earthq Eng 2017;99:97–107.
[27] Bojórquez E, Iervolino I. Spectral shape proxies and nonlinear structural response. Soil Dyn Earthq Eng 2011;31(7):996–1008.
[28] Jamshidiha H, Yakhchalian M, Mohebi B. Advanced scalar intensity measures for collapse capacity prediction of steel moment resisting frames with fluid viscous dampers. Soil Dyn Earthq Eng 2018;109:102–18.
[29] Boore DM. Orientation-independent, nongeometric-mean measures of seismic intensity from two horizontal components of motion. Bull Seismol Soc Am 2010;100(4):1830–5.
[30] Baker JW, Cornell CA. Which spectral acceleration are you using? Earthq Spectra 2006;22(2):293–312.
[31] Kottke A. Pyrotd v0.5.4. Zenodo; 2018, http://dx.doi.org/10.5281/zenodo.1322849.
[32] Reed JW, Kassawara RP. A criterion for determining exceedance of the operating basis earthquake. Nucl Eng Des 1990;123(2–3):387–96.
[33] Cordova PP, Deierlein GG, Mehanny SS, Cornell CA. Development of a two-parameter seismic intensity measure and probabilistic assessment procedure. In: The second US-Japan workshop on performance-based earthquake engineering methodology for reinforced concrete building structures, Vol. 20. 2000.
[34] Vamvatsikos D, Cornell CA. Developing efficient scalar and vector intensity measures for IDA capacity estimation by incorporating elastic spectral shape information. Earthq Eng Struct Dynam 2005;34(13):1573–600.
[35] Housner GW. Behavior of structures during earthquakes. J Eng Mech Div 1959;85(4):109–29.
[36] Von Thun JL. Earthquake ground motions for design and analysis of dams. In: Earthquake engineering and soil dynamics II-Recent advances in ground-motion evaluation. ASCE; 1988.
[37] Bradley BA. Empirical equations for the prediction of displacement spectrum intensity and its correlation with other intensity measures. Soil Dyn Earthq Eng 2011;31(8):1182–91.
[38] Arias A. Measure of earthquake intensity. Technical report, Massachusetts Inst. of Tech., Cambridge. Univ. of Chile, Santiago de Chile; 1970.
[39] FEMA. Short-period building collapse performance and recommendations for improving seismic design. FEMA P-2139-2, vol. 2 - Study of one-to-four story wood light-frame buildings, Washington, D.C.: Federal Emergency Management Agency; 2020.
[40] Mazzoni S, McKenna F, Scott MH, Fenves GL, et al. OpenSees command language manual, vol. 264. Berkeley, California, United States: Pacific Earthquake Engineering Research (PEER) Center; 2006.
[41] Folz B, Filiatrault A. Cyclic analysis of wood shear walls. J Struct Eng 2001;127(4):433–41.
[42] Lowes LN, Mitra N, Altoontash A. A beam-column joint model for simulating the earthquake response of reinforced concrete frames. Pacific Earthquake Engineering Research Center, (PEER); 2003.
[43] Welch D, Deierlein G, Reis E, Burton H. Quantifying the benefit of retrofitting unbraced cripple walls in single-family wood-frame dwellings. In: Proceedings of the 17th World Conference on Earthquake Engineering, Japan. 2020.
[44] Dahal L, Burton H, Yi Z. An end-to-end computational platform to automate seismic design, nonlinear analysis, and loss assessment of woodframe buildings. In: 12th national conference in earthquake engineering. 2022.
[45] Guan X, Burton H, Sabol T. Python-based computational platform to automate seismic design, nonlinear structural model construction and analysis of steel moment resisting frames. Eng Struct 2020;224:111199.
[46] Miranda E, Bertero VV. Evaluation of strength reduction factors for earthquake-resistant design. Earthq Spectra 1994;10(2):357–79.
[47] Dahal L, Burton H, Onyambu S. Quantifying the effect of probability model misspecification in seismic collapse risk assessment. Struct Saf 2022;96:102185.
[48] Ghasemi A, Zahediasl S. Normality tests for statistical analysis: A guide for non-statisticians. Int J Endocrinol Metabol 2012;10(2):486.